

Supersolidity in the second layer of *para*-H₂ adsorbed on graphite

M. C. Gordillo

*Departamento de Sistemas Físicos, Químicos y Naturales,
Facultad de Ciencias Experimentales, Universidad Pablo de Olavide,
Carretera de Utrera km 1, E-41013 Sevilla, Spain*

J. Boronat

Departament de Física, Universitat Politècnica de Catalunya, Campus Nord B4-B5, 08034 Barcelona, Spain

(Dated: March 8, 2022)

We calculated the phase diagram of the second layer of *para*-H₂ adsorbed on graphite using quantum Monte Carlo methods. The second layer shows an incommensurate triangular crystal structure. By using a symmetric wave function, that makes possible molecule exchanges, we observed that this nearly two-dimensional crystal shows a finite superfluid density around a total density of 0.1650 Å⁻². The superfluid fraction of this supersolid phase was found to be small, 0.41±0.05 %, but still experimentally accessible.

I. INTRODUCTION

The study of the adsorption of quantum gases on graphite is a venerable area of study (see for instance Ref. 1 and references therein), dating back to the 80's and 90's of the past century. A set of calorimetric, torsional oscillator, and neutron diffraction works helped to define the phase diagrams both of the first and second helium²⁻⁶ and, to a lesser extent, molecular hydrogen layers⁷⁻¹⁴ on top of that substrate. Those studies have recently been complemented by measurements on the adsorption of ⁴He on the outer surface of carbon nanotubes^{15,16}, introducing curvature effects in the layer formation.

In spite of this long period of intense study, some recent experimental work shows that the nature of the second ⁴He layer on graphite was not perfectly understood. Refs. 17 and 18 hinted at the existence of novel superhexatic and supersolid phases, in addition to the well established translationally invariant and triangular incommensurate solid. The supersolidity claim was sustained both by an independent set of torsional oscillator measurements¹⁹ and by a theoretical calculation on the same system²⁰. Both works seem to point to a registered two-dimensional (2D) crystal phase with a superfluid fraction appreciably above zero. Ref. 20 proposed that phase to be a 7/12 solid, commensurate with the triangular solid of the first layer.

Surprisingly, this is not the only work in which ⁴He is proposed to form a supersolid phase. Ref. 21 shows that a registered $\sqrt{3} \times \sqrt{3}$ arrangement on the first layer adsorbed on graphite had a non-negligible but tiny superfluid fraction of 0.67 %. The same calculation repeated for H₂ under the same conditions produced a normal solid. On the other hand, a strictly 2D H₂ system was found to be supersolid in the range between the spinodal and the equilibrium densities²². However, the superfluid densities were also quite small.

para-H₂ has been deeply studied both theoretically and experimentally searching for a new superfluid. Its

light mass makes it a priori a good candidate that could sum up to the paradigmatic case of helium. However, its molecule-molecule interaction is much more attractive than helium, hindering the formation of a bulk liquid. To date, there is only evidence of superfluid signal in some spectroscopic studies of small doped H₂ droplets^{23,24}, in agreement with several theoretical calculations²⁵⁻³⁰. It was also shown that a metastable H₂ glass has a critical temperature $T_c \simeq 1$ K, with a superfluid fraction below 1%³¹.

In this work, we explore the possibility of the second layer of H₂ adsorbed on graphite to be a supersolid. By a supersolid we mean a system that is not translationally invariant but that has a non-zero superfluid fraction. In this way, it would joint the list of known setups with those characteristics that today includes, besides quasi two-dimensional ⁴He^{18,19}, some cold gas arrangements³²⁻³⁴. To do so, we solve the Schrödinger equation that describes the system using the first-principles diffusion Monte Carlo (DMC) method. Our study, restricted to the $T = 0$ limit, shows that the stable phase corresponding to the second layer of H₂ grown on top of the first solid layer is an incommensurate triangular crystal for all the coverages. Our results for the superfluid fraction of this solid show a small density island, around the lowest density of the second layer, where its value is different from zero. Even if this range is small and the superfluid fraction is predicted to be tiny, its value is under reach using modern torsional oscillator designs¹⁹.

II. METHOD

The DMC method is a stochastic technique that allows us to obtain the ground state of a zero-temperature system of bosons, as the *para*-H₂ molecules considered in this work³⁵. DMC solves exactly the N -body Schrödinger equation in imaginary time, within some statistical er-

rors. The Hamiltonian of the system under study is

$$H = \sum_{i=1}^N \left[-\frac{\hbar^2}{2m} \nabla_i^2 + V_{\text{ext}}(x_i, y_i, z_i) \right] + \sum_{i<j}^N V_{\text{H}_2-\text{H}_2}(r_{ij}). \quad (1)$$

Here, x_i , y_i , and z_i are the coordinates of each one of the N H_2 molecules with mass m located both on the first and second layers. Since we considered a full corrugated substrate, we have to sum up all the C- H_2 interactions, represented by $V_{\text{ext}}(x_i, y_i, z_i)$. The functional form of the C- H_2 potential³⁶ was the same as in a previous work for the same system on graphene³⁷. The carbon atoms were located in the graphite crystallographic positions in the standard way, positions that were kept fixed. The intermolecular potential $V_{\text{H}_2-\text{H}_2}$ is the Silvera and Goldman potential³⁸, a staple in these kinds of calculations, that depends only on the distance between the center of masses of each pair of para- H_2 molecules, r_{ij} , and not on their relative orientations (spherical molecules). Its expression is, in atomic units:

$$V(r_{ij}) = \exp(1.713 - 1.5671r_{ij} - 0.00993r_{ij}^2) - \left(\frac{12.14}{r_{ij}^6} + \frac{215.2}{r_{ij}^8} + \frac{4813.9}{r_{ij}^{10}} - \frac{143.1}{r_{ij}^9} \right) f(r_{ij}). \quad (2)$$

where $f(r_{ij}) = \exp(-(1.28r_m/r_{ij} - 1)^2)$ for $r_{ij} < 1.28r_m$ and 1 otherwise, with $r_m = 3.44 \text{ \AA}$.

In order to reduce the statistical variance of the simulations and to fix the system phase, DMC uses an initial approximation to the many-body wave function which acts as guiding drive along the diffusion process. In the present study we used

$$\Phi(\mathbf{r}_1, \dots, \mathbf{r}_N) = \Phi_J(\mathbf{r}_1, \dots, \mathbf{r}_N) \Phi_1(\mathbf{r}_1, \dots, \mathbf{r}_{N_1}) \times \Phi_2(\mathbf{r}_{N_1+1}, \dots, \mathbf{r}_N), \quad (3)$$

with

$$\Phi_J(\mathbf{r}_1, \dots, \mathbf{r}_N) = \prod_{i<j}^N \exp \left[-\frac{1}{2} \left(\frac{b}{r_{ij}} \right)^5 \right] \quad (4)$$

a Bijl-Jastrow wave function that depends on b , a variationally optimized parameter whose value was found to be 3.195 \AA , in agreement with a previous calculation in a similar system³⁷. The expression for Φ_1 was

$$\Phi_1(\mathbf{r}_1, \mathbf{r}_2, \dots, \mathbf{r}_{N_1}) = \prod_i^{N_1} \prod_J^{N_C} \exp \left[-\frac{1}{2} \left(\frac{b_C}{r_{iJ}} \right)^5 \right] \times \prod_i \exp \{ -c_1 [(x_i - x_{\text{site},i})^2 + (y_i - y_{\text{site},i})^2] \} \times \prod_i^{N_1} \exp(-a_1(z_i - z_1)^2), \quad (5)$$

where N_1 is the number of molecules in the first layer, and r_{iJ} represents the distance between the center or mass of each molecule, i , and each of the N_C carbon atoms, J ,

in the graphite crystal. The coordinates $(x_{\text{site}}, y_{\text{site}})$ are the crystallographic positions of the 2D triangular first layer lattice. The variational parameters in Eq. (5) were optimized and found to be the same as the ones in Ref. 37, i.e., $a_1 = 3.06 \text{ \AA}^{-2}$, $b_C = 2.3 \text{ \AA}$, $z_1 = 2.9 \text{ \AA}$. The parameter c_1 was obtained from linear interpolation between the values corresponding to densities in the range 0.08 \AA^{-2} ($c_1 = 0.61 \text{ \AA}^{-2}$) and 0.10 \AA^{-2} ($c_1 = 1.38 \text{ \AA}^{-2}$) obtained in a previous calculation including only the first layer³⁹. If in Eq. (3) we assume $\Phi_2 = 1$, we are dealing only with the first layer.

On the other hand, the study of the second layer is carried out by taking Φ_2 as

$$\Phi_2(\mathbf{r}_{N_1+1}, \dots, \mathbf{r}_N) = \prod_i^{N_2} \prod_J^{N_C} \exp \left[-\frac{1}{2} \left(\frac{b_C}{r_{iJ}} \right)^5 \right] \times \prod_{i=1}^{N_2} \left[\sum_{J=N_1+1}^N \exp \{ -c_2 [(x_i - x_{\text{site},I})^2 + (y_i - y_{\text{site},I})^2] \} \right] \times \prod_i^{N_1} \exp(-a_2(z_i - z_2)^2) \quad (6)$$

N_2 being the number of molecules in the second layer ($N = N_1 + N_2$), $a_2 = 1.52 \text{ \AA}^{-2}$ and $z_2 = 6 \text{ \AA}$. The parameter c_2 was interpolated as in Φ_1 . The points $(x_{\text{site}}, y_{\text{site}})$ are again the crystallographic positions of a 2D lattice, but now for the second layer. This symmetrized Nosanow wave function allows for possible exchanges in the crystal²⁰, something essential to have superfluidity. When we wanted to have a second-layer liquid, we fixed c_2 to zero. The use of an un-symmetrized trial function similar to Eq. 5 to describe the second layer produces always higher energies than the ones obtained by using the above equation.

All the data presented in this work are the result of the average of 10 independent Monte Carlo histories for each density and for all of the simulation cells used. A history is a set of $1.2 \cdot 10^5$ Monte Carlo steps, each step involving the change in the positions, according to the prescription of the diffusion Monte Carlo algorithm³⁵, of all the molecules in each of the 300 walkers (configurations) needed to describe the systems under consideration. To increase the number of Monte Carlo steps, the number of walkers or the number of independent histories do not vary the results shown. Of those $1.2 \cdot 10^5$ Monte Carlo steps, the first $2 \cdot 10^4$ were ignored in the calculation of averages. Further increases in the length of the stories did not improve neither the values nor the error bars of the averages obtained. The number of molecules per configuration oscillated between 216 and 356, depending on the size of the simulation cell. That meant 144 and 224 molecules in the first layer, respectively. In the solid or supersolid arrangements no vacancies were included. To avoid mismatch problems with the incommensurate arrangements in the second and first layers, both were considered to be at the center a nine-cell structure created by replication of the original cell by the vectors defined

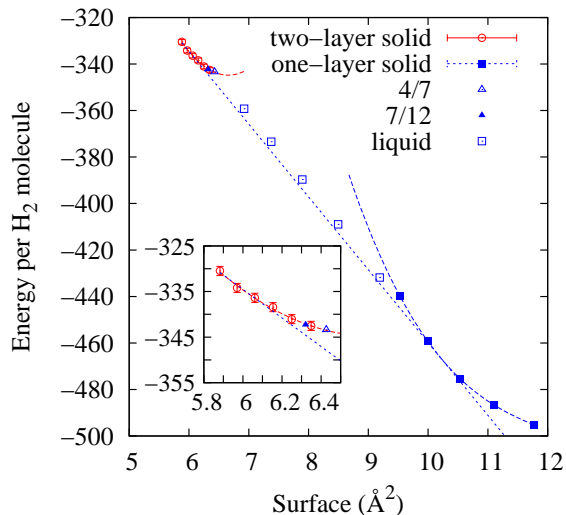


FIG. 1. Energy per H_2 molecule as a function of the inverse of the total density of H_2 on graphite. The dotted line represent the Maxwell construction to determine the transition densities from a one-layer system to a two-layer arrangement. The curves are polynomial fits to the data and are intended only as guides-to-the-eye. The inset is a zoom on the two-layer solid energies.

by their length and width. Only the interactions within a given distance of the molecules in the original simulation cell were considered in the Monte Carlo averages. We checked that the averages for all the magnitudes presented here were independent of the size and shape of simulation cell, what implies that this replicating procedure avoids any problems derived from the incommensurability of the first and second layers.

III. RESULTS

The first relevant issue is establishing the stability limits of the different phases of H_2 adsorbed on graphite. This was done to ascertain whether there was any substantial difference with the phase diagram of the second layer of H_2 on graphene dealt with in Ref. 37. To do so, we calculated the energies per molecule for the different arrangements we have considered, i.e., a first-layer triangular crystal and a second-layer with two possibilities: liquid and a triangular incommensurate solid on top of another triangular incommensurate solid in the first layer. As indicated above, those results are the average of at least 10 Monte Carlo histories for each density. To avoid spurious correlations, only values located 100 Monte Carlo steps away were used to obtain the mean energies. Our DMC results are shown in Fig. 1. The double-tangent Maxwell construction line indicates that one-layer incommensurate solid of $0.097 \pm 0.002 \text{ \AA}^{-2}$ is in equilibrium with two stacked triangular incommensu-

rate crystals of total density $0.1650 \pm 0.0025 \text{ \AA}^{-2}$, as can be better seen in the inset of that figure. The density of the first layer was 0.100 \AA^{-2} , density at which the total energy of the entire arrangement was found to be the lowest one. This density translates to a H_2 - H_2 lattice constant of 3.4 \AA . Those results are in good agreement with the ones for graphene³⁷. Apart from the values of the equilibrium densities, the main features of Fig. 1 coincide with both the graphene calculation and available experimental data¹¹, i.e., there are no stable second-layer liquid nor registered commensurate solids of the second layer with respect the first one (either $4/7$ or $7/12$) since, in both cases, the energies are above the Maxwell line. A picture of those commensurate arrangements can be found in Refs. 40 and 41, respectively.

The low mass of the H_2 molecule makes it a good candidate to exhibit macroscopic quantum behavior. To explore this possibility, we studied if we could find a supersolid phase within the stability range of the second-layer triangular solid. We chose H_2 on top of H_2 , on top of graphite, because the supersolidity of the first layer had been ruled out in a previous calculation²¹. Following the same procedure as in Ref. 18 for ^4He adsorbed on graphite, we estimated the superfluid fraction in two dimensions ρ_s/ρ of H_2 in the second layer by using the zero-temperature winding number estimator,

$$\frac{\rho_s}{\rho} = \lim_{\tau \rightarrow \infty} \alpha \left(\frac{D_s(\tau)}{\tau} \right), \quad (7)$$

with τ the imaginary time used in the quantum Monte Carlo simulation. Here, $\alpha = N_2/(4D_0)$, $D_0 = \hbar^2/(2m)$, and $D_s(\tau) = \langle [\mathbf{R}_{CM}(\tau) - \mathbf{R}_{CM}(0)]^2 \rangle$. \mathbf{R}_{CM} is the position of the center of mass of the N_2 H_2 molecules located in the second layer. To perform those calculations, we took into account only their x and y coordinates, where periodic boundary conditions apply. The results obtained for a system with a total density of 0.1650 \AA^{-2} are displayed in Fig. 2. There, we show $\alpha D_s(\tau)$ vs. τ , the superfluid fraction being the slope of the curve for $\tau \rightarrow \infty$. As one can see in Fig. 2, ρ_s/ρ is noticeable different from zero, i.e., the system is a supersolid at that density.

To be sure that this result did not depend on our choosing of any particular setup, and to be sure that there were no influence of any possible sluggishness in the superfluid estimator, we performed DMC simulations using three different simulation cells. For instance, a 14×8 simulation cell is made of 14 first-layer unit cells in the x direction, and of 8 of those unit cells in the y direction. Since, as mentioned before, the distance between H_2 molecules in that first layer is 3.4 \AA , this means a $47.6 \times 47.11 \text{ \AA}^2$ simulation cell. Conversely, the dimensions of a 12×6 cell are $40.8 \times 35.33 \text{ \AA}^2$. This implies a surface ratio between both setups of ~ 1.55 . The superfluid estimator (7) was calculated as the average of ten statistically independent simulations and displayed in Fig. 2 as a thin line. No obvious size trend was found, the values for the three simulation cells being remarkably close to each other. In fact, the open squares in that figure

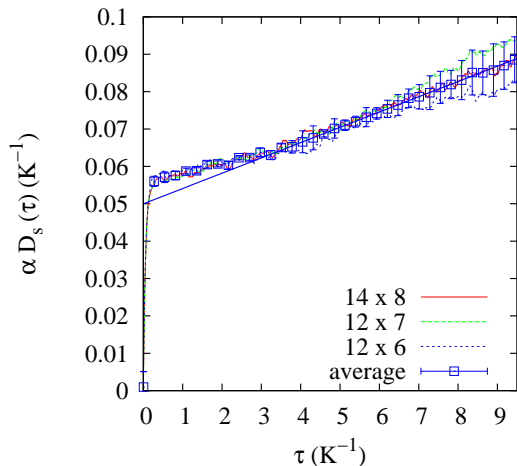


FIG. 2. Estimator of the superfluid density for a total density $\rho = 0.1650 \text{ \AA}^{-2}$ for different sizes of the simulation cell expressed as multiples of a single unit cell in the first layer. Lines, simulation results; open squares, average of all the estimator for the three cells displayed. The straight line represent a linear least-squares fit to the the symbols displayed in the range ($3 < \tau < 8 \text{ K}^{-1}$). The slope of that curve implies a superfluid density of $0.41 \pm 0.05 \%$.

represent the average of the three of them for each τ , the error bars corresponding to two standard deviations of that average and including all the values obtained in the simulations.

To obtain the superfluid fraction, we performed a least-squares linear fitting procedure to the average of $\alpha D_s(\tau)$ vs. τ for the three simulation cells considered. The τ values were in the range $3 < \tau < 8 \text{ K}^{-1}$. The result is displayed as the thick continuous line in Fig. 2. The procedure produces an slope, corresponding to the superfluid fraction, of $0.41 \pm 0.05 \%$. If instead of using the average of $\alpha D_s(\tau)$ as an input in the fitting procedure, we consider the values for each simulation cell separately, we get superfluid fractions of $0.36 \pm 0.05 \%$ for the 12×6 cell, $0.48 \pm 0.05 \%$ for the 12×7 cell, and $0.39 \pm 0.05 \%$ for the 14×7 cell. Larger cells are beyond our calculating capabilities. These values are of the same order as the superfluid fraction obtained for the metastable, strictly 2D, systems considered in Ref.²². According to the results displayed in Fig. 1, the arrangement with a

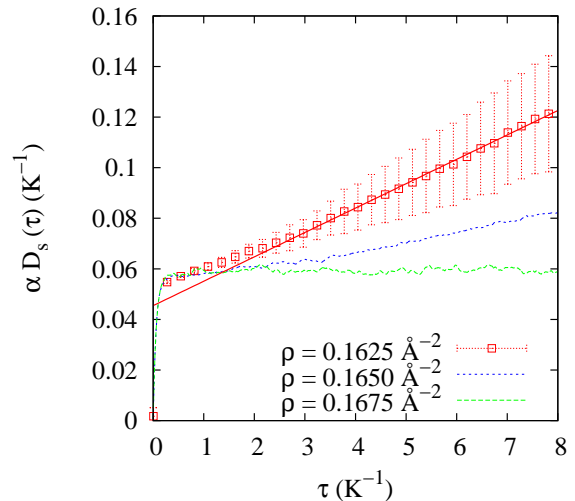


FIG. 3. Same as in Fig. 2, but for different total densities and a fixed 14×8 simulation cell. The slope for the density $\rho = 0.1625 \text{ \AA}^{-2}$ implies a superfluid fraction of $0.96 \pm 0.05 \%$. Error bars are only shown for the lower density to make the figure more clear; for the other two densities they are of the same size.

total density of 0.1650 \AA^{-2} is stable, and thus we can conclude that this supersolid could be observed. We can also see that the least-squares fit also describes well the interval $\tau > 8 \text{ K}^{-1}$, indicating that no further lengthening of the simulation series is necessary to obtain an accurate value of the superfluid fraction.

To check the density range in which that supersolid phase could be stable, we calculated the superfluid fraction (Eq. 7) for total densities of 0.1625 \AA^{-2} (metastable) and 0.1675 \AA^{-2} . We did not consider the $4/7$ and $7/12$ unstable phases since their corresponding densities (0.157 and 0.158 \AA^{-2} respectively) are too far away from the stability region. The results are shown in Fig. 3 for a 14×8 simulation cell. We observe that, for the lower density, there is an appreciable superfluid fraction of $0.96 \pm 0.05 \%$. However, in the other case corresponding to the higher density, the slope of the estimator is zero, implying that the second layer of H_2 at that density is a normal solid.

IV. CONCLUSIONS

Summarizing, our microscopic quantum Monte Carlo approach shows that there is a narrow density slice around 0.1650 \AA^{-2} in which an incommensurate triangular second-layer H_2 supersolid is stable. We can try to understand the reasons behind this somehow unexpected result. The first ingredient is undoubtedly the low density of the crystal considered. That second-layer density is 0.0650 \AA^{-2} . However, this is larger than the 0.060 \AA^{-2} upper density limit for which you can see a

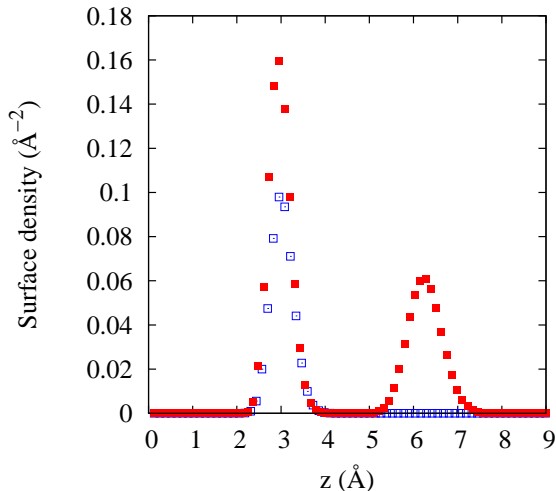


FIG. 4. Density profile in the direction perpendicular to the graphite plane. Open squares, density corresponding to a first-layer commensurate $\sqrt{3} \times \sqrt{3}$ structure; full squares, a two-layer system of total density $\rho = 0.1650 \text{ \AA}^{-2}$.

superfluid fraction in a pure 2D crystal²² and also larger than the 0.0636 \AA^{-2} first layer density for which no superfluid was found in Ref. 21. Therefore, an additional factor is needed. That factor can be understood with the help of Fig. 4. There, we show the density profile of a $\sqrt{3} \times \sqrt{3}$ first layer registered phase, together with the double layer supersolid arrangement in a direction perpendicular (z) to the graphite plane. What we can see is that there is an appreciable difference between the z -width of the first (bare or with H_2 on top) and second H_2 layers. In particular, the ratio between their widths, estimated considering the first- and second-layer profiles as Gaussians, is about 1.5. This implies a considerably larger leeway for the molecules in the second layer to move, and to allow for the exchanges needed to create a superfluid. That is corroborated by the superfluidity

fraction of $0.58 \pm 0.05 \%$ obtained for a second layer of H_2 of the same density adsorbed on top of a first layer of D_2 . The second-layer density profile in this case is virtually identical to the presented in Fig. 4 and not shown for simplicity. This means that the origin of this feature is in the transverse displacement of the molecules in the second layer.

The only remaining and crucial issue would be about the possibility of detecting such a small superfluid fraction. In a very recent experimental work¹⁹, this is shown to be feasible for a double layer of ^4He on top of graphite, since they were able to detect fractions as small as 0.9%. Importantly, the temperatures at which that behavior was seen in ^4He are well below 0.5 K, what makes us confident that our zero-temperature DMC results for H_2 would hold in future experiments to come. Incidentally, we should say that a very recent calculation⁴² points out to the existence of a supersolid in a quite different, but related system, bulk D_2 at very high pressures.

ACKNOWLEDGMENTS

We acknowledge financial support from MCIN/AEI/10.13039/501100011033 (Spain) Grants PID2020-113565GB-C22 and PID2020-113565GB-C21, from Junta de Andalucía group PAIDI-205, and the UPO-FEDER grant UPO-1380159. J. B. acknowledges financial support from Secretaria d'Universitats i Recerca del Departament d'Empresa i Coneixement de la Generalitat de Catalunya, co-funded by the European Union Regional Development Fund within the ERDF Operational Program of Catalunya (project Quantum-Cat, ref. 001-P-001644). We also acknowledge the use of the C3UPO computer facilities at the Universidad Pablo de Olavide.

¹ L.W. Bruch, M.W. Cole, and E. Zaremba. *Physical Adsorption, Forces and Phenomena* (Dover, New York, 1997).
² D. S. Greywall and P. A. Busch, *Phys. Rev. Lett.* **67**, 3535 (1991).
³ D. S. Greywall, *Phys. Rev. B* **47**, 309 (1993).
⁴ G. Zimmerli, G. Mistura, and M. H. W. Chan, *Phys. Rev. Lett.* **68**, 60 (1992).
⁵ P. A. Crowell and J. D. Reppy, *Phys. Rev. Lett.* **70**, 3291 (1993).
⁶ P. A. Crowell and J. D. Reppy, *Phys. Rev. B* **53**, 2701 (1996).
⁷ H. Freimuth and H. Wiechert, *Surf. Sci.* **162**, 432 (1985).
⁸ H. Freimuth and H. Wiechert, *Surf. Sci.* **189/190**, 548 (1987).
⁹ J. Ma, D. L. Kingsbury, F. C. Liu, and O. E. Vilches, *Phys. Rev. Lett.* **61**, 2348 (1988).

¹⁰ J. Cui and S.C. Fain Jr., *Phys. Rev. B.* **39** 8628 (1989).
¹¹ H. Wiechert, in *Excitations in Two-Dimensional and Three-Dimensional Quantum Fluids* edited by A.G.F. Wyatt and H.J. Lauter (Plenum Press, New York, 1991). p. 499.
¹² O.E. Vilches, *J. Low Temp. Phys.* **89**, 267 (1992).
¹³ W. Liu and S.C. Fain Jr., *Phys. Rev. B* **47**, 15965 (1993).
¹⁴ F. C. Liu, Y. M. Liu, and O. E. Vilches, *Phys. Rev. B* **51**, 2848 (1995).
¹⁵ A. Noury, J. Vergara-Cruz, P. Morfin, B. Placais, M. C. Gordillo, J. Boronat, S. Balibar, and A. Bachtold, *Phys. Rev. Lett* **122**, 165301 (2019).
¹⁶ Emin Menachekanian, Vito Iaia, Mingyu Fan, Jingjing Chen, Chaowei Hu, Ved Mittal, Gengming Liu, Raul Reyes, Fufang Wen, and Gary A. Williams *Phys. Rev. B* **99**, 064503 (2019).

- ¹⁷ S. Nakamura, K. Matsui, T. Matsui, and H. Fukuyama, Phys. Rev. B **94**, 180501(R) (2016).
- ¹⁸ J. Nyéki, A. Phillis, A. Ho, D. Lee, P. Coleman, J. Parpia, B. Cowan, and J. Saunders, Nature Phys. **13**, 455 (2017).
- ¹⁹ Jaewon Choi, Alexey A. Zadorozhko, Jeakyung Choi, and Eunseong Kim, Phys. Rev. Lett. **127**, 135301 (2021).
- ²⁰ M. C. Gordillo and J. Boronat, Phys. Rev. Lett. **124**, 205301 (2020).
- ²¹ M. C. Gordillo, C. Cazorla, and J. Boronat, Phys. Rev. B **83**, 121406(R) (2011).
- ²² C. Cazorla and J. Boronat, Phys. Rev. B **78**, 134509 (2008).
- ²³ S. Grebenev, B. Sartakov, J. P. Toennies, and A. F. Vilesov, Science **289**, 1532 (2000).
- ²⁴ H. Li, R. J. Le Roy, P. N. Roy, and A. R. W. McKellar, Phys. Rev. Lett. **105**, 133401 (2010).
- ²⁵ P. Sindzingre, D. M. Ceperley, and M. L. Klein, Phys. Rev. Lett. **67**, 1871 (1991).
- ²⁶ M.C. Gordillo. Phys. Rev. B **60** 6790 (1999).
- ²⁷ M.C. Gordillo and D.M. Ceperley. Phys. Rev. B **65**, 174527 (2002).
- ²⁸ F. Mezzacapo and M. Boninsegni, Phys. Rev. Lett. **100**, 145301 (2008).
- ²⁹ E. Sola and J. Boronat, J. Phys. Chem. A **115**, 7071 (2011).
- ³⁰ Y. Kwon and K.B. Whaley. Phys. Rev. Lett. **89** 273401 (2002).
- ³¹ O. N. Osychenko, R. Rota, and J. Boronat, Phys. Rev. B **85**, 224513 (2012).
- ³² J. Léonard, A. Morales, P. Zupancic, T. Esslinger, and T. Donner, Nature (London) **543**, 87 (2017),
- ³³ J. Li, J. Lee, W. Huang, S. Burchesky, B. Shteynas, F. Top, A. Jamison, and W. Ketterle, Nature (London) **543**, 91 (2017),
- ³⁴ L. Tanzi, E. Lucioni, F. Fama, J. Catani, A. Fioretti, C. Gabbanini, R.N. Bisset, L. Santos, and G. Modugno, Phys. Rev. Lett. **122**, 130405 (2019).
- ³⁵ J. Boronat, in *Microscopic Approaches to Quantum Liquids in Confined Geometries*, Vol. 4, ed. E. Krotscheck and J. Navarro (World Scientific, Singapore, 2002).
- ³⁶ G. Stan and M. W. Cole, J. Low Temp. Phys. **110**, 539 (1998).
- ³⁷ M. C. Gordillo and J. Boronat. Phys. Rev. B **87**, 165403 (2013).
- ³⁸ I. F. Silvera and V. V. Goldman, J. Chem. Phys. **69**, 4209 (1978).
- ³⁹ M.C. Gordillo and J. Boronat. Phys. Rev. B **81**, 155435 (2010).
- ⁴⁰ H. Fuyuyama. J. Phys. Soc. Japan **77** 111013 (2008).
- ⁴¹ Y. Kwon and D.M. Ceperley. Phys. Rev. B **85** 224501 (2012).
- ⁴² C. W. Myung ,B. Hirshberg, and M. Parrinello Phys. Rev. Lett. **128** 045301 (2022).